Acta Crystallographica Section D
Biological Crystallography
ISSN 0907-4449

X-ray crystal structure and small-angle X-ray scattering of sheep liver sorbitol dehydrogenase

Hemant Yennawar,[a] Magda Møller,[b,c] Richard Gillilan[b] and Neela Yennawar[a]*

[a]Department of Biochemistry and Molecular Biology and Huck Institutes of Life Sciences, Pennsylvania State University, 8 Althouse Laboratory, University Park, PA 16802, USA, [b]Macromolecular Diffraction Facility, Cornell High Energy Synchrotron Source, Ithaca, NY 14853, USA, and [c]Department of Medicinal Chemistry, Faculty of Pharmaceutical Sciences, University of Copenhagen, DK-2100 Copenhagen, Denmark

Correspondence e-mail: nhy1@psu.edu

Received 26 January 2011
Accepted 1 March 2011

PDB Reference: sheep liver sorbitol dehydrogenase, 3qe3.

The X-ray crystal structure of sheep liver sorbitol dehydrogenase (slSDH) has been determined using the crystal structure of human sorbitol dehydrogenase (hSDH) as a molecular-replacement model. slSDH crystallized in space group *I*222 with one monomer in the asymmetric unit. A conserved tetramer that superposes well with that seen in hSDH (despite belonging to a different space group) and obeying the 222 crystal symmetry is seen in slSDH. An acetate molecule is bound in the active site, coordinating to the active-site zinc through a water molecule. Glycerol, a substrate of slSDH, also occupies the substrate-binding pocket together with the acetate designed by nature to fit large polyol substrates. The substrate-binding pocket is seen to be in close proximity to the tetramer interface, which explains the need for the structural integrity of the tetramer for enzyme activity. Small-angle X-ray scattering was also used to identify the quaternary structure of the tetramer of slSDH in solution.

1. Introduction

Sorbitol dehydrogenase (SDH) and aldose reductase form the polyol pathway that interconverts glucose and fructose and hence are important enzymes in diabetic research (Li *et al.*, 2008; Oates, 2002). Redox changes from overproduction of the coenzyme nicotinamide adenine dinucleotide (NAD) by SDH may play a role in diabetes-related complications, thus making SDH a therapeutic target. Crystal structures of this important enzyme have previously been determined from silverleaf whitefly (PDB entry 1e3j; Banfield *et al.*, 2001), human (hSDH; PDB entries 1pl6, 1pl7 and 1pl8; Pauly *et al.*, 2003) and *Rhodobacter sphaeroides* (PDB entry 1k2w; Philippsen *et al.*, 2005). None of these structures are of a complex with a substrate. We now report the crystal structure of sheep liver SDH with a substrate bound in the active site (PDB code 3qe3). Our structure does not include the coenzyme NAD. Earlier biochemical studies on SDH have shown it to only be functional when present in a tetrameric quarternary structure (Hellgren *et al.*, 2007). The crystal structure that we report offers details of the tetramer interactions and shows the proximity of the substrate-binding pocket to the tetramer interface. Small-angle X-ray scattering (SAXS) verifies the tetramer disposition in solution. Comparison of the sheep liver and human SDH structures (87% identity) has led us to model a ternary

complex of SDH with the NAD cofactor and sorbitol, a natural substrate.

2. Materials and methods

2.1. X-ray crystal structure

Sheep liver SDH (slSDH) was purchased from Sigma and used with no further purification. The enzyme was crystallized using the nonphotochemical laser-induced nucleation technique with the commercially available PEG/Ion screen from Hampton Research. This crystallization screening method has been described by Yennawar *et al.* (2010). Crystals grown at pH 7.0 from 0.2 *M* lithium acetate dihydrate and 20% polyethylene glycol 3350 were used for data collection. The crystals were soaked for 10 min with 10% glycerol in the mother liquor before cryofreezing to 93 K. X-ray diffraction was observed to a resolution of 1.8 Å. The diffraction data were collected at the home laboratory (Penn State) on a Rigaku MicroMax-007 rotating-anode generator equipped with a Saturn 944+ CCD detector and an X-stream 2000 for cryocooling. The data were processed using the *CrystalClear* software suite (Rigaku Corp.) as well as *HKL*-2000 (Otwinowski & Minor, 1997). The structure was obtained by molecular replacement using the hSDH model (PDB entry 1pl8) in the program *Phaser* (McCoy *et al.*, 2007). The crystals belonged to space group *I*222, with a monomer in the asymmetric unit. TLS refinement using the *PHENIX* program (Adams *et al.*, 2010) alternated with visualization of the model and electron-density fitting using *Coot* (Emsley & Cowtan, 2004) completed the crystal structure solution. Model analysis was performed using *PyMOL* (v.1.3; Schrödinger LLC). There is electron density in the active site for the catalytic zinc, an acetate molecule and a glycerol molecule (Fig. 1). Data-collection and refinement parameters are listed in Table 1.

To explore the aggregation of slSDH in solution, we used dynamic light scattering (Viscotek 802 from Malvern Instruments and the associated *OmniSIZE* software). The estimated size and molecular weight were determined to be about 5 nm and 152 kDa, respectively, suggesting a tetrameric species. In order to obtain the exact quaternary structure of the tetramer in solution, the following SAXS studies were undertaken.

Table 1
Data-collection and refinement statistics.

Values in parentheses are for the outer shell.

Data collection	
Space group	*I*222
Unit-cell parameters (Å)	a = 67.77, b = 85.92, c = 119.92
Resolution (Å)	1.9 (1.93–1.9)
Measured reflections	113512
Unique reflections	27906 (1386)
R_{merge} (%)	12.6 (59.3)
$\langle I/\sigma(I)\rangle$	9.455 (1.16)
Completeness (%)	99.6 (100)
Average multiplicity	4.1 (3.0)
Overall Wilson B value for data (Å^2)	21.0
Refinement	
Resolution range (Å)	34.4–1.9
Unique reflections	27886
Reflections in test set (5%)	1416
R_{cryst} (%)	18.6
R_{free} (%)	23.2
R.m.s.d. bond lengths† (Å)	0.007
R.m.s.d. bond angles† (°)	1.046
No. of non-H protein atoms	2638
No. of Zn atoms	1
No. of glycerol molecules	1
No. of acetates	3
No. of water molecules	214
Mean B factors (Å^2)	
Protein	30.8
Zn	50.4
Glycerol molecules	41.1
Acetates	56.4
Waters	37.5

† Calculated for the protein using ideal values (Engh & Huber, 1991).

2.2. SAXS data collection

slSDH solutions at concentrations of 20, 16 and 10 mg ml^{-1} were prepared at each of the pH values 7.0, 9.4, 9.6, 10.4 and 10.6 used for the SAXS analysis. Buffer containing 0.2 *M* glycine–NaOH was used for pH 9.4, 9.6, 10.4 and 10.6, while 0.1 *M* HEPES was used for pH 7.0. The protein solution was centrifuged at 14 000 rev min^{-1} for 10 min prior to data collection. SAXS data were collected on CHESS beamline F2 at 9.881 keV (1.2563 Å, the tantalum edge). The X-ray beam was collimated to 250 × 250 µm and was centered on a 2 mm diameter vertical quartz capillary tube with 10 µm thick walls (Hampton Research, Aliso Viejo, California, USA). The capillary tube and full X-ray flight path, including beamstop, were kept *in vacuo* to eliminate air scatter. Sample plugs of approximately 15–20 µl were delivered from a 96-well plate to the capillary using a Hudson SOLO single-channel pipetting robot (Hudson Robotics Inc., Springfield, New Jersey, USA). To reduce radiation damage, the sample plugs were oscillated in the X-ray beam using a computer-controlled syringe pump (Aurora Biomed, Vancouver,

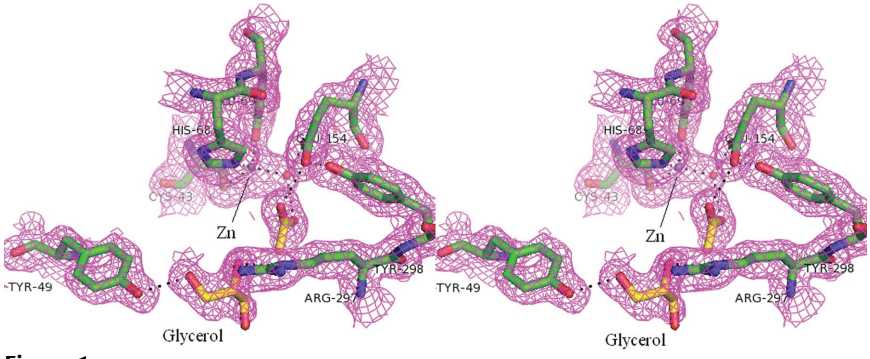

Figure 1
Stereoview of the active site with bound acetate and glycerol molecules. Glycerol is a substrate of SDH. The electron density shown is an OMIT map excluding the zinc, glycerol and acetate and contoured at the 1.0σ level. Zinc-coordination and hydrogen-bond interactions are marked as black dotted lines (distances less than 3.2 Å). The present structure lacks the NAD cofactor in the active site.

Canada). Images were collected on a Quantum 1 CCD detector (Area Detector Systems Corporation, Poway, California, USA) with sequential 180 s exposures being used to assess possible radiation damage. The sample-to-detector distance was calibrated using silver behenate powder (The Gem Dugout, State College, Pennsylvania, USA). CCD images were reduced to profiles and buffer-subtracted using the *BioXTAS RAW* software (Nielsen *et al.*, 2009). While the useful q-space range [$q = 4\pi\sin(\theta)\lambda$, with 2θ being the scattering angle] was determined on a case-by-case basis using the Guinier plot as a guide, it was generally the case that $q_{\min} = 0.02$ Å^{-1} and $q_{\max} = 0.24$ Å^{-1}.

Typically, samples at each pH setting were measured at three different concentrations, 20, 16 and 10 mg ml^{-1}, in order to determine the extent of interparticle interference and concentration effects. Owing to sample limitations, only two concentrations were collected at each end of the pH range. For pH 7.0, samples at 10 and 20 mg ml^{-1} were collected. Superposition of the two intensity curves in this case has been provided in the Supplementary Material[1] (Fig. S1). The radius of gyration (R_g) was calculated using both the method of Guinier (Guinier & Fourne, 1955) and the inverse Fourier transform (IFT) method as implemented in the *GNOM* program (Semenyuk & Svergun, 1991). In the case of the Guinier method, linear fitting was performed on data having a range of $qR_g < 1.3$ unless otherwise noted. Interactive fitting was performed using the *BioXTAS RAW* program (Nielsen *et al.*, 2009). IFT methods are thought to be less sensitive to radiation-induced aggregation and concentration effects; consequently, comparison of the R_g values obtained using the Guinier and IFT methods gives a useful indication of quality and error range. The maximum diameter of the protein ($D_{\max}$) was determined by plotting the total estimate scores (Svergun, 1992) and χ^2 for a range of $D_{\max}$ values using the *RunGnomRun* script (Hura *et al.*, 2009).

The experimental SAXS data were compared with the crystal structure of slSDH using the program *CRYSOL* (Svergun *et al.*, 1995). The program calculates a scattering curve for a given atomic structure and fits it to the experimental scattering curve. The SAXS data were analyzed for the presence of different oligomeric states of the protein and different conformations of possible oligomers in the solution using the program *OLIGOMER* (Konarev *et al.*, 2003). The program provides the volume fractions of each component in the solution by fitting the experimental curve to a multicomponent mixture of possible protein oligomers and oligomer conformations given to the program. The scattering form factors for likely oligomeric states and conformations were calculated using the program *CRYSOL*. The R_g values required by *OLIGOMER* were calculated using *CRYSOL*, while the molecular weight (dimer = 75.66 kDa, tetramer = 151.32 kDa) was based on sequence information.

Shape reconstruction was performed by running ten independent *DAMMIF* calculations (Franke & Svergun, 2009) and building a consensus model using the *DAMAVER* program (Volkov & Svergun, 2003). No symmetry conditions were imposed on the solutions.

3. Results and discussion

3.1. Crystal structure

The overall fold and active-site configuration of slSDH are similar to those in previously reported hSDH crystal structures. The r.m.s. deviation for superposition of 324 C$^{\alpha}$ atoms between the hSDH (PDB entry 1pl6) and slSDH monomers is 0.51 Å. In the following discussion, residues lining the active site are conserved in slSDH and hSDH.

3.2. Active site of slSDH

The catalytic zinc is coordinated by the three residues His68, Cys43 and Glu69 and a water molecule (Fig. 1). The zinc is coordinated to an acetate molecule through the water molecule. The acetate occupies part of the putative substrate-binding pocket. The acetate interaction through a water molecule differs from the direct interaction seen between the inhibitor 4-[2-(hydroxymethyl)pyrimidin-4-yl]-*N,N*-dimethylpiperazine-1-sulfonamide and zinc in the hSDH structure 1pl6 (Pauly *et al.*, 2003). Details of the interactions of the zinc are shown in Fig. 1.

The large substrate-binding pocket of the active site has a bound glycerol molecule adjacent to the acetate molecule (Fig. 1). The glycerol hydrogen bonds to four polar residues lining the substrate-binding pocket: Glu154, Tyr298, Arg297 and Tyr49. These residues show a small reorganization with respect to their counterparts in the human structures lacking the substrate. In addition to these, residues Phe58, Phe296 and Phe117 in the surrounding region show a slight reorientation in their side-chain conformations. The substrate pocket is large enough to accommodate larger polyol substrates. Glycerol has been studied as a substrate of SDH (Lindstad *et al.*, 1998; Lindstad & McKinley-McKee, 1993). The present crystal structure does not include the bound coenzyme NAD, hence allowing glycerol to remain in the active site without undergoing any chemical reaction. In the present structure, the cofactor-binding pocket is occupied by a total of seven water molecules. The side chains of residues Glu276, Leu273, Val251 and Arg207 lining the cofactor-binding pocket show subtle changes in slSDH compared with the hSDH and NAD complex structures. Previous studies have suggested that the cofactor binds first before substrate binding. The absence of the cofactor in the present structure may have led to the lack of direct coordination of the substrate glycerol to the zinc.

3.3. Model of the ternary complex

Based on the glycerol- and acetate-binding positions seen in the present structure and the cofactor binding in the complex structures of hSDH, we propose a model for binding of the natural substrate sorbitol and the NAD cofactor in Fig. 2. In

[1] Supplementary material has been deposited in the IUCr electronic archive (Reference: HM5096). Services for accessing this material are described at the back of the journal.

this figure the orientation of the sorbitol has been optimized for proton abstraction from the C2 carbon by the cofactor. The modelling protocol has changed the orientation of the carboxamide group on NAD^+ with respect to the pyridine ring. The sorbitol hydroxyl provides the fifth coordination site for the Zn atom. Similar to the glycerol interactions in our structure, residues Glu154, Arg297 and Tyr49 hydrogen bond to the hydroxyl groups of the sorbitol.

3.4. Quaternary structure

slSDH crystallized in space group *I*222 with a monomer in the asymmetric unit. In the case of hSDH the space group was $P6_2$ with a tetramer in the asymmetric unit. The crystal packing of slSDH differs from that of hSDH, but both have superimposable tetramer configurations with an r.m.s. deviation on superposition of 0.59 Å (1051 C^{α} atoms) and a buried surface area of about 2796 $Å^2$. The conserved tetramer fits best to the solution tetramer structure observed in the SAXS experiment. Previous mutation studies have shown that an intact tetramer is crucial for biological activity (Hellgren *et al.*, 2007). As seen in Fig. 3, the tetramer interface forms the structural scaffold to stabilize the substrate-binding pocket. The tetramer is held together by several hydrogen bonds and hydrophobic interactions. In Fig. 3(*a*) each monomer is coloured differently. The top pair in blue and magenta form one dimer unit. This dimer, along with the second dimer shown in green and red, forms the tetramer.

3.4.1. Dimer. Two monomers related by twofold symmetry form a closely packed dimer, with a β-sheet hydrogen bond traversing across the monomers at residue Ile292 (Fig. 3). Within each monomer the β-sheet has a parallel architecture, while the two β-strands at the interface are antiparallel. The residues interacting at the monomer boundary are Arg108, Asn110, His161, Ile292, Phe296 and Arg165 of one monomer and Gly265, Glu289, Asp291 and Ile292 of the other monomer (Fig. 3*b*). The residue Phe296 contributing to the dimer interface is adjacent to residues Arg297 and Tyr298 of the substrate-binding pocket. The side chain of Phe296 is 4.0 Å from a glycerol hydroxyl. Surface representations show that the dissociation of the dimer compromises the integrity of the substrate tunnel leading to the active site and leaves the residues of the substrate-binding pocket with more flexibility.

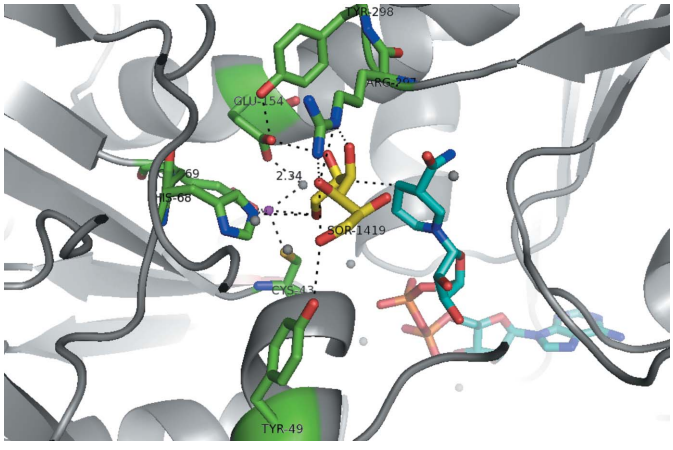

Figure 2
A model of NAD and sorbitol binding as guided by the present and human SDH structures.

3.4.2. Tetramer. The tetramer is formed by a dimer of dimers and has 222 point-group symmetry that coincides with the crystallographic 222 symmetry of the slSDH crystals. The tetramer assembly is a result of hydrogen-bonding interactions between Glu102 and Lys105 of one dimer and Tyr139 and Asn300 of the second dimer (Fig. 3*c*; residues 102 and 105 of the green monomer interact with residues 139 and 300 of the magenta monomer, and residues 102 and 105 of the blue monomer interact with residues 139 and 300 of the red monomer in Fig. 3*a*) and a reciprocal interaction from the second dimer to the first (residues 102 and 105 of the magenta monomer interact with residues 139 and 300 of the green monomer, and residues 102 and 105 of the red monomer interact with residues 139 and 300 of the blue monomer in Fig. 3*a*). The side chains of Leu170 reside in a hydrophobic pocket across the dimer interface (Leu170 of the green monomer into the hydrophobic pocket of the blue monomer and *vice versa* in Figs. 3*a* and 3*d*; Leu170 of the magenta monomer into the hydrophobic pocket in the red monomer and *vice versa* in Fig. 3*a*). Just as in the case of the proximity of the monomer–monomer interface to the substrate glycerol, Asn300 contributing to the dimer–dimer interface is one residue away from the substrate-binding pocket residues Arg297 and Tyr298. The side chain of Tyr298 is spatially surrounded by the side chains of Asn300, Tyr109, Gln93 (Glu in hSDH) and Tyr139, which interact with each other by a hydrogen-bond network. This network must have been destabilized when Tyr109 was mutated to Phe, causing disruption of the dimer–dimer interface and a reduction in activity (Hellgren *et al.*, 2007).

3.5. SAXS structure

Applying crystallographic symmetry operations from the *I*222 space group to the monomer in the asymmetric unit generated two plausible tetrameric configurations of slSDH monomers. The first tetramer model (tetramer 1) is structurally equivalent to the tetramer found in the asymmetric unit of hSDH. The second model (tetramer 2) has a slightly more extended configuration (Fig. 4*a*). Using coordinates from the slSDH structure, the radius of gyration R_g was calculated for monomer (21.4 Å), dimer (30.5 Å), tetramer 1 (33.7 Å) and tetramer 2 (38.51 Å) models. The solution R_g behavior determined for slSDH over a range of concentrations and pH values is relatively flat at both high and low pH values, but rises sharply in the intermediate pH range (Supplementary Fig. S2). The change from a tetramer to a higher oligomer at around pH 10.0 corresponds to the pK_a of a tyrosine residue side-chain hydroxyl. Mutation studies (Hellgren *et al.*, 2007) had indicated Tyr110 as being crucial for tetramer stability. It is possible that once the tetramer falls apart the monomers might associate in a nonspecific manner to form larger clusters.

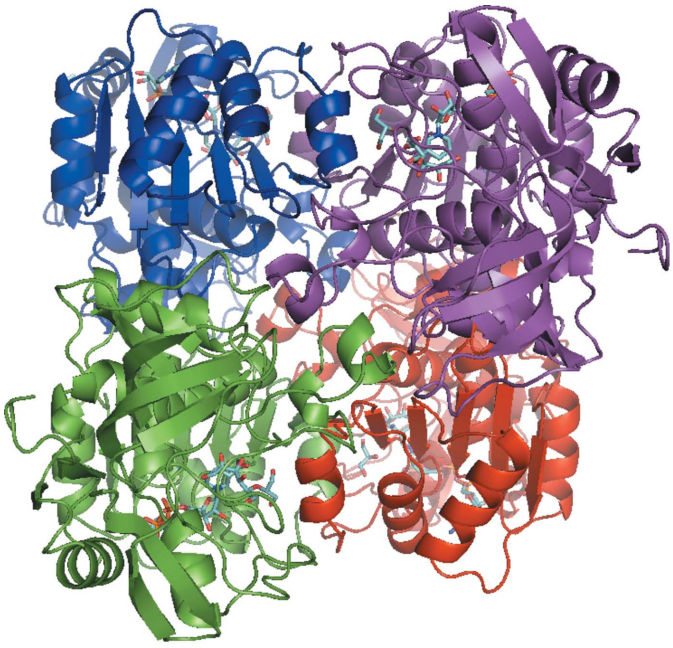

(*a*)

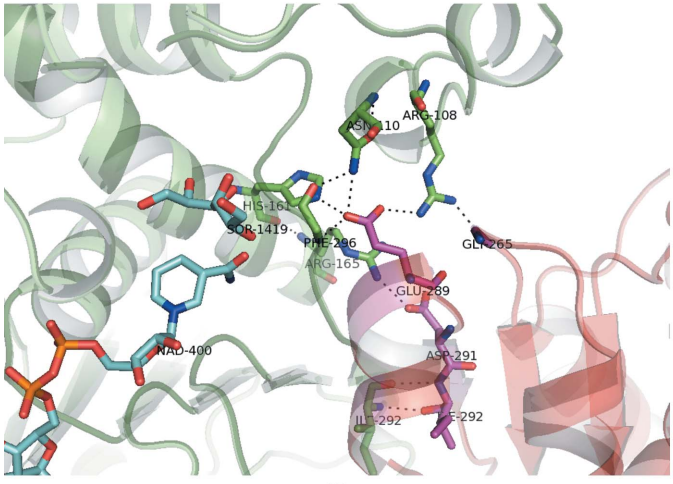

(*b*)

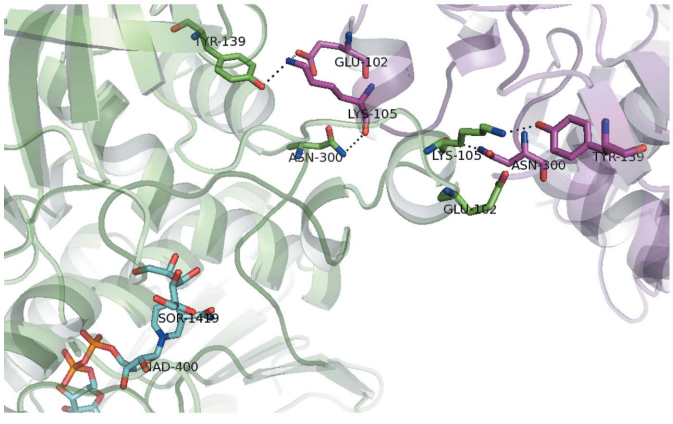

(*c*)

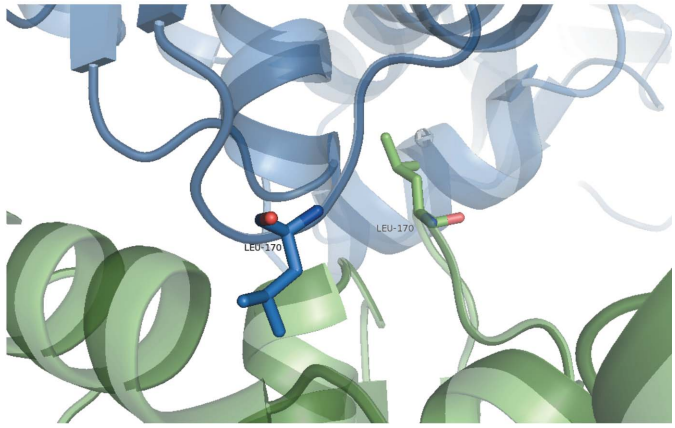

(*d*)

In all cases the Guinier plots displayed clear linear behavior, although at higher pH values it was not possible to maintain $qR_g < 1.3$ with this particular beamline configuration. The R_g value at pH 7.0 is 33.0 ± 0.6 Å, which suggests that the solution state of slSDH is predominantly tetramer 1 (R_g = 33.74) at low pH with a transition to higher oligomeric states at higher pH values. See Supplementary Fig. S3 for a plot of the Guinier range of data at pH 7.0. The intensity plots for the two available pH 7.0 concentrations (10 and 20 mg ml^{-1}) overlay to within experimental error (Supplementary Fig. S3). SAXS data collected at 20 mg ml^{-1} were used for further analysis.

Kratky plots show folded behavior in all cases, although at pH 7.0 and pH 10.4 there is some rise in the plots at the widest angles (Supplementary Fig. S4). Since most other plots display falling behavior in this range, we chose to confine most of our analysis of the pH 7.0 data to a lower resolution range of $q <$ (0.15), where the noise arising from low signal, normalization errors and minor structural disorder is less significant. For *DAMMIF* models we used a wider angle range of $q < 0.2$.

Theoretical scattering profiles generated from the dimer and tetramer models using the *CRYSOL* program (Svergun *et al.*, 1995) show a clear preference for tetramer 1 (χ^2 = 0.73) over tetramer 2 (χ^2 = 1.4) (Fig. 4*b*). A calculation using the *OLIGOMER* program, which computes volume fractions of known components, is more informative. Supplementary Table S1 gives the computed volume fractions of various proposed combinations of dimer, tetramer 1 and tetramer 2. In all cases preference is given to tetramer 1 over tetramer 2 and dimer.

The maximum diameter D_{max} of the IFT curve for the pH 7.0 data is 87 Å (Supplementary Fig. S5). The R_g value as calculated in real space by the IFT method is 32.95 ± 0.1 Å. The R_g values estimated using the Guinier approach (33.0 ± 0.6 Å) are in good agreement with those from the IFT method.

Low-resolution shape reconstructions using the *DAMMIF* and *DAMAVER* programs (Volkov & Svergun, 2003; Franke

Figure 3
A number of van der Waals contacts and hydrogen bonds stabilize the dimer and tetramer interfaces. Tetramer formation is crucial to strengthen the substrate-binding pockets, shown here occupied by a model of sorbitol (SOR1419) in cyan. A stick model of the NADH cofactor is shown in cyan. (*a*) The tetramer as seen in the crystal packing of human and sheep liver SDH crystal structures. (*b*) Interactions seen within a dimer; each monomer forms crucial hydrogen bonds to complete the substrate-binding pocket of the other monomer. (*c*, *d*) Interactions seen across dimers.

& Svergun, 2009) produced models having an average NSD (normalized spatial discrepancy) value of 0.589, indicating a stable reconstruction. Alignment of the tetramer models and envelope using the *SUPCOMB*20 program (Kozin & Svergun, 2001) yielded NSDs of 1.03 for tetramer 1 and 1.25 for tetramer 2. Tetramer 1 is therefore the favored oligomeric state configuration for slSDH in solution.

To conclude, this is the first report comparing the crystal and solution structures of sheep liver sorbitol dehydrogenase. The crystal structure describes a complex of the enzyme and glycerol and shows details of the interactions with the substrate. Strong binding forces help the four subunits of the enzyme to come together to form a tight tetramer whose interface is in proximity to the substrate-binding pocket. This finding provides a unique structural explanation of the enzyme's activity as a tetramer. Of the two possible tetramer states seen *via* crystal packing, the SAXS study picks the one that is seen in solution.

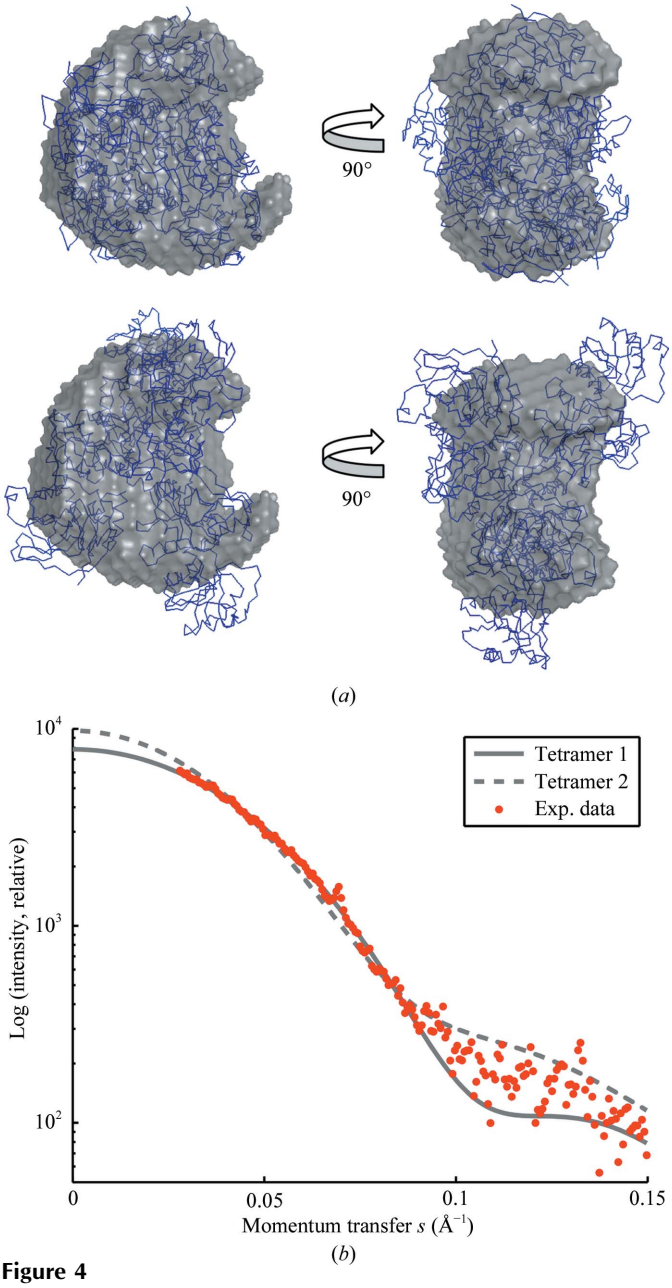

Figure 4
(*a*) SAXS envelopes superimposed on two candidate tetramers derived from crystal lattice symmetry. Tetramer 1 (top) is structurally analogous to the asymmetric unit of hSDH and is reasonably well contained by the experimental envelope. Tetramer 2 (bottom) is less compact and is not well contained by the envelope. (*b*) Computed *versus* experimental scattering for tetramer models. Tetramer 1 most closely matches the experimental data in the region $q < 0.1$ Å.

We would like to acknowledge the NIH–NCRR shared instrumentation grant 1S10RR023439-01 to NHY. We would also like to thank Drs Gopalan and Denev from the PSU Centre for Optical Technologies for help with crystallization of slSDH using the laser. This project was funded in part by a grant from the Pennsylvania Department of Health using Tobacco Settlement Funds. MM thanks Bente Vestergaard for supervision and is grateful for financial support from the Faculty of Pharmaceutical Sciences, University of Copenhagen and the Bioxtas project group with funding from the NABITT program of the Danish Ministry of Science, Technology and Development (grant No. 2106-050047). This work is based in part upon research conducted at the Cornell High Energy Synchrotron Source (CHESS), which is supported by the National Science Foundation and the National Institutes of Health/National Institute of General Medical Sciences under NSF award DMR-0936384, using the Macromolecular Diffraction at CHESS (MacCHESS) facility, which is supported by award RR-01646 from the National Institutes of Health through its National Center for Research Resources.

References

Adams, P. D. *et al.* (2010). *Acta Cryst.* D**66**, 213–221.
Banfield, M. J., Salvucci, M. E., Baker, E. N. & Smith, C. A. (2001). *J. Mol. Biol.* **306**, 239–250.
Emsley, P. & Cowtan, K. (2004). *Acta Cryst.* D**60**, 2126–2132.
Engh, R. A. & Huber, R. (1991). *Acta Cryst.* A**47**, 392–400.
Franke, D. & Svergun, D. I. (2009). *J. Appl. Cryst.* **42**, 342–346.
Guinier, A. & Fourne, G. (1955). *Small-Angle Scattering of X-rays.* New York: John Wiley & Sons.
Hellgren, M., Kaiser, C., de Haij, S., Norberg, A. & Höög, J. O. (2007). *Cell. Mol. Life Sci.* **64**, 3129–3138.
Hura, G. L., Menon, A. L., Hammel, M., Rambo, R. P., Poole, F. L., Tsutakawa, S. E., Jenney, F. E., Classen, S., Frankel, K. A., Hopkins, R. C., Yang, S., Scott, J. W., Dillard, B. D., Adams, M. W. & Tainer, J. A. (2009). *Nature Methods*, **6**, 606–612.
Konarev, P. V., Volkov, V. V., Sokolova, A. V., Koch, M. H. J. & Svergun, D. I. (2003). *J. Appl. Cryst.* **36**, 1277–1282.
Kozin, M. B. & Svergun, D. I. (2001). *J. Appl. Cryst.* **34**, 33–41.
Li, Q., Hwang, Y. Y. C., Ananthakrishnan, R., Oates, P. J., Guberski, D. & Ramasamy, R. (2008). *Cardiovasc. Diabetol.* **7**, 33.
Lindstad, R. I., Köll, P. & McKinley-McKee, J. S. (1998). *Biochem. J.* **330**, 479–487.
Lindstad, R. I. & McKinley-McKee, J. S. (1993). *FEBS Lett.* **330**, 31–35.
McCoy, A. J., Grosse-Kunstleve, R. W., Adams, P. D., Winn, M. D., Storoni, L. C. & Read, R. J. (2007). *J. Appl. Cryst.* **40**, 658–674.
Nielsen, S. S., Toft, K. N., Snakenborg, D., Jeppesen, M. G., Jacobsen, J. K., Vestergaard, B., Kutter, J. P. & Arleth, L. (2009). *J. Appl. Cryst.* **42**, 959–964.
Oates, P. J. (2002). *Int. Rev. Neurobiol.* **50**, 325–392.
Otwinowski, Z. & Minor, W. (1997). *Methods Enzymol.* **276**, 307–326.

Pauly, T. A. *et al.* (2003). *Structure*, **11**, 1071–1085.
Philippsen, A., Schirmer, T., Stein, M. A., Giffhorn, F. & Stetefeld, J. (2005). *Acta Cryst.* D**61**, 374–379.
Semenyuk, A. V. & Svergun, D. I. (1991). *J. Appl. Cryst.* **24**, 537–540.
Svergun, D. I. (1992). *J. Appl. Cryst.* **25**, 495–503.
Svergun, D., Barberato, C. & Koch, M. H. J. (1995). *J. Appl. Cryst.* **28**, 768–773.
Volkov, V. V. & Svergun, D. I. (2003). *J. Appl. Cryst.* **36**, 860–864.
Yennawar, N., Denev, S., Gopalan, V. & Yennawar, H. (2010). *Acta Cryst.* F**66**, 969–972.